Available online at www.sciencedirect.com
SCIENCE DIRECT®
ELSEVIER
Journal of Magnetism and Magnetic Materials 269 (2004) 359–371
Journal of magnetism and magnetic materials
www.elsevier.com/locate/jmmm

Development of pulsed magnetic field and study of magnetotransport properties of K-doped $La_{1-x}Ca_{x-y}K_yMnO_3$ CMR materials

Sayani Bhattacharya[a], Sudipta Pal[a], R.K. Mukherjee[a], B.K. Chaudhuri[a,*], S. Neeleshwar[b], Y.Y. Chen[b], S. Mollah[c], H.D. Yang[c]

[a] *Department of Solid State Physics, Indian Association for the Cultivation of Science, Kolkata 700032, India*
[b] *Institute of Physics, Academia Sinica, Taipei, Taiwan, ROC*
[c] *Department of Physics, National Sun Yat Sen University, Kaohsiung 804, Taiwan, ROC*

Received 4 March 2003; received in revised form 18 July 2003

Abstract

Temperature-dependent magnetization, magnetoresistance and magneto-thermoelectric power of the K doped $La_{1-x}Ca_{x-y}K_yMnO_3$ type samples with $x = 0.3$ and $0 \leqslant y \leqslant 0.15$ has been studied. All the samples exhibit sharp metal–insulator transition (MIT) around T_p accompanied by a ferromagnetic (metallic) to paramagnetic (semiconducting) phase transition with a well-defined Curie temperature T_C (almost equal to T_p). Doping of monovalent K in the divalent Ca site of $La_{1-x}Ca_{x-y}K_yMnO_3$ drives the system from a high resistivity regime with lower T_p to a lower resistivity regime with higher T_p. Systematic increase of Curie temperature with increase of K doing is observed from the magnetization measurement down to 5 K. Low temperature resistivity (ρ) and thermoelectric power (Seebeck coefficient, S) data well fit the relations $\rho = \rho_0 + \rho_2 T^2$ and $S = S_0 + S_{3/2}T^{3/2} + S_4 T^4$, respectively, signifying the importance of electron–magnon scattering process ($\rho_2 T^2$ and $S_{3/2}T^{3/2}$ term). On the other hand, the high temperature ($T > T_p$ upto 320 K) conductivity data satisfy the variable range hopping (VRH) model. For $T > 320$ K small polaron hopping model is more appropriate than the VRH model. High temperature thermoelectric power (TEP) data also indicates the formation of thermally activated small polarons. Even with very small change of y, the density of states at the Fermi level $N(E_F)$ changes considerably. The magnetotransport properties have been measured under pulsed magnetic field of microsecond duration. The decay time of the magnetic pulse within the sample (t) varies with field strength, which indicates that with change of magnetic field, ordering of the spin in the ferromagnetic regime changes.

PACS: 71.38.+i; 71.30.+h; 75.30.Vn

Keywords: Pulse magnetic field; K doping; Electron–magnon

1. Introduction

Colossal magnetoresistivity (CMR) in manganites is an example in which spin, charge and

*Corresponding author. Tel.: +91-33-247-34971; fax: +91-33-247-32805.
E-mail address: sspbkc@mahendra.iacs.res.in (B.K. Chaudhuri).

0304-8853/$ - see front matter © 2003 Elsevier B.V. All rights reserved.
doi:10.1016/S0304-8853(03)00632-2

lattice degrees of freedom conspire to produce a dramatic effect. This system exhibits many significant properties like metal–insulator transition (MIT), ferromagnetic (FM)—paramagnetic (PM) phase change, charge and orbital ordering (CO and OO), etc. depending on the charge density, temperature and atomic structure. Zener proposed that the spin structure and the electronic properties of $R_{1-x}A_xMnO_3$ (R = rare earth metal, A = divalent element) were correlated via the double-exchange (DE) mechanism controlled by the motion of the e_g electrons from Mn^{3+} to Mn^{4+} sites [1]. However, Millis et al. [2] argued that the physics of manganites is dominated by the interplay between a strong electron–phonon coupling and the large Hund coupling effect that optimizes the electronic kinetic energy by the generation of a FM phase. Theoretically, they proved that the effective coupling $\lambda_{eff}(= E_{JT}/t_{eff})$ dominates the physics of the manganites, where E_{JT} is the static trapping energy and t_{eff} is an effective hopping that is temperature-dependent following *DE*. Above the Curie temperature (T_C), λ_{eff} could be greater than the critical value that leads to insulating behavior due to electron localization (caused by the splitting of the degenerate e_g levels at MnO_6 octahedra). Below T_C, λ_{eff} becomes smaller than the critical value and hence metallic behavior is induced. Moreover, other factors viz. average sizes of the R and A site cations, mismatch effect, vacancy in R and Mn sites and the oxygen stoichiometry [3] also play a crucial role. Till now, most of the studies had been concentrated on the divalent ion doped $R_{1-x}A_xMnO_3$ (A = Ca, Sr, Pb, Ba, etc.) compounds and many of these samples crystallize in an orthorhombically distorted perovskite structure (O′-type; $c/2 < a < b$; space group Pbmn) with a cooperative ordering of Jahn–Teller distorted $Mn^{3+}O_6$ octahedra [4]. In contrast, there are only few reports of monovalent alkali-metal ion doped compounds [5–8]. Monovalent alkali doping on $LaMnO_3$ can lead to different consequences. Because of the larger valence difference between La^{3+} and alkali-metal ions [7], fewer impurity ions (K ions) are needed to achieve a specific carrier concentration and larger random-potential fluctuations are experienced by the electrons in the σ^*-bond. Consequently, it will cause less inhomogeneity. Since the valence state of the alkali-metal ions is +1, substitution of these ions affect the ratio of $Mn^{3+}(t_{2g}^3e_g^1 : S = 2)$ and $Mn^{4+}(t_{2g}^3e_g^0$: $S = 3/2)$ ions which ultimately also affects the DE mechanism.

In this paper, we have used pulsed magnetic field of short duration to study the transport properties of the selected samples, which gives identical results with those obtained under DC magnetic field. Earlier Date [9] used a single pulse to study magnetization and resistivity at different magnetic field. Obviously, the advantage of the pulsed field technique is that one can measure transport and magnetic properties low and high magnetic fields, using relatively an easy process without using superconducting magnet. Moreover, in the present experimental setup, data can be collected within very short interval of time so that heating effect due to eddy current is not very effective [9].

In this work, we have prepared a novel manganite series $La_{1-x}Ca_xMnO_3$ where Ca^{2+} ions have been partially replaced by K^+ ions. Experimental data both in the high temperature ($T > T_p$) and low temperature ($T < T_p$) phases have been analyzed with theoretical models used in our earlier work [10,11]. Momentary excitation of the magnetic spins with pulsed field and the corresponding time of their return to the normal state (relaxation time) has also been measured indicating spin ordering in the sample.

2. Experimental

2.1. Sample preparation

$La_{1-x}Ca_{x-y}K_yMnO_3$ type samples (with $x = 0.3$ and $y = 0.0$, 0.05, 0.1, 0.15) were prepared by a standard ceramic processing technique [12]. Well-mixed stoichiometric mixtures of La_2O_3, CaO, K_2CO_3 and $(CH_3COO)_2Mn$, $4H_2O$ (each of purity >99%) were first heated to 773 K and then to 1073 K for 5 h with intermediate grinding and then again annealing at 1173 K for 48 h. The sintered powder thus obtained was ground, palletized and annealed again at 1073 K for 72 h and then furnace cooled to room temperature. X-ray powder diffraction study has been made with CuK_α

radiation for structural study and the magnetization of the samples are measured by a SQUID magnetometer in the temperature range 4–300 K.

2.2. Arrangement for resistivity measurement under pulsed magnetic field

For the magnetoresistance study under pulsed field, we used a lab-made setup of a pulsed magnetic field produced in an air-core solenoid coil by sudden discharge of a capacitor bank (Fig. 1). The sample was mounted on the tail-end part of the modified closed cycle helium cryostat (Displex, Air Products). For good electrical contacts gold electrodes (films) were first made on the sample surface by vacuum sputtering technique and the electrical contacts of the leads and the sample were made with good-quality quickly drying silver paints. To avoid the induction effect (spurious) that arises due to the introduction of a low resistive sample into the magnetic field, data were taken at the peak of the pulsed field where induction effect is zero. The sample placed nearly at the center of the solenoid coil feels a pulsed magnetic field in a vertical direction whenever a surge of current passes through the coil. The capacitor voltage is changed with the help of a variac to get different magnetic field strengths. In the present case, we have measured with a maximum magnetic field of 3.2 T and between 350 and 15 K. The peak value of the magnetic field is measured utilizing the procedure discussed elsewhere [12]. To minimize the heating effect due to eddy current produced by pulse field, the sample was mounted in parallel to the direction of magnetic field so that the effective area of the sample perpendicular to the field is very small [9].

3. Results and discussion

3.1. Structural studies with X-ray diffraction

X-ray powder diffraction (XRD) data of the samples at room temperature were recorded in a Philips PW1710 diffractometer using CuK_{α} radiation with Ni filter. The XRD pattern of two samples one without K ($y = 0.0$) and the other

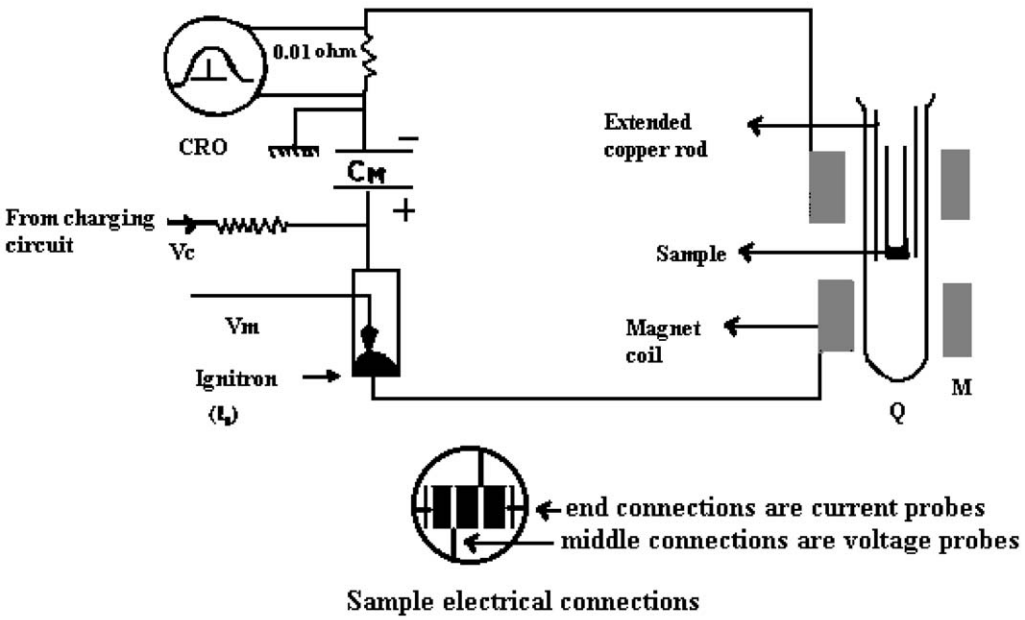

Fig. 1. Circuit diagram for pulsed magnetic field generation. M: Magnet coil, C_M: Main capacitor and Q: Quartz tube, CRO: Digital storage oscilloscope.

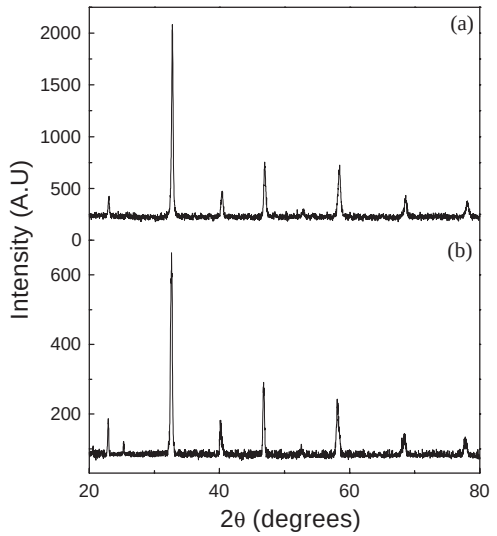

Fig. 2. XRD pattern of the sample $La_{1-x}Ca_{x-y}K_yMnO_3$ taken at room temperature with CuK_α radiation: (a) with $x = 0.3$ and $y = 0.0$ and (b) with $x = 0.3$ and $y = 0.15$.

Table 1
Crystallographic data of $La_{0.7}Ca_{0.3-y}K_yMnO_3$

y	a (Å)	b (Å)	c (Å)	α (deg)	Structure
0.0	5.47	7.736	5.497	—	Orthorhombic (Pbmn)
0.05	5.46	7.728	5.501	—	Orthorhombic (Pnma)
0.10	5.50	—	—	60.32	Rhombohedral (R $\bar{3}$c)
0.15	5.54	—	—	60.27	Rhombohedral (R $\bar{3}$c)

with 15% K substitutions are shown in Fig. 2(a) and (b), respectively. It is clear from the diffraction pattern that the synthesized samples are single phase with no measurable impurity phases. Structural analyses of the samples were performed using the program DBWS. The refined values of the structural parameters are given in Table 1. It was observed that the undoped sample ($y = 0.0$) and the sample with 5% potassium shows an orthorhombic perovskite structure. Space group Pbmn and Pnma were, respectively, used in the refinement whereas, R $\bar{3}$c space group in the hexagonal axes was used for the other two K doped samples. It is clear from the analysis that K doping induces rhombohedral distortion, which is consistent with the previously reported results [5,6]. The transition from the orthorhombic phase to the rhombohedral phase due to K doping indicates that structural disorder decreases and hence Mn–O–Mn bond angle increases. The distortion in the MnO_6 octahedron becomes less with the Mn–O–Mn bond angle moving towards 180°. Less distortion in the crystal structure reduces the possibility of charge localization and hence samples become more conducting, which is further supported by resistivity data. In this regard it should be mentioned that Roy et al. [8] have shown that for the $La_{1-x}Na_xMnO_3$ systems, increased Na doping drives the structure to become more cubic, resulting in an increase of the one-electron bandwidth. Consequently, the possibility of greater overlapping is increased and hence greater conductivity is observed.

3.2. Magnetic properties

Fig. 3(a) shows the temperature-dependent magnetization (M) obtained in the zero-field-cooled (ZFC) and field-cooled (FC) processes with an applied field of 0.01 T for two typical samples ($y = 0.0$ and 0.10). The ZFC curve indicates the samples undergo a paramagnetic (PM) to FM phase transition and like T_p (discussed later), the Curie temperature T_C also increases with increasing K doping. This is explained by considering that with increasing K doping concentration (y), the ratio of Mn^{4+}/Mn^{3+} increases (discussed later) which favors the ferromagnetic DE interaction. The number of ferromagnetically aligned domains supercedes the paramagnetically aligned background and hence percolation threshold is attained with increasing K doping. Hence the compound becomes FM throughout the temperature range. We also see from the data that magnetization almost saturates for $y \geqslant 0.1$ and the net magnetic moment decreases with further increase of y (Fig. 3(b)). Almost similar result was explained by Roy et al. [8] as the completion of rhombohedral phase for $y \geqslant 0.1$ that contributes to the magnetization. In the high doping regime the increase in Mn^{4+} ions favors the antiferromagnetic super-exchange interaction (Mn^{4+}–O–Mn^{4+}) over the DE interaction and hence magnetization decreases. The FC and ZFC data do not coincide at low temperatures indicating the presence of some randomly frozen in

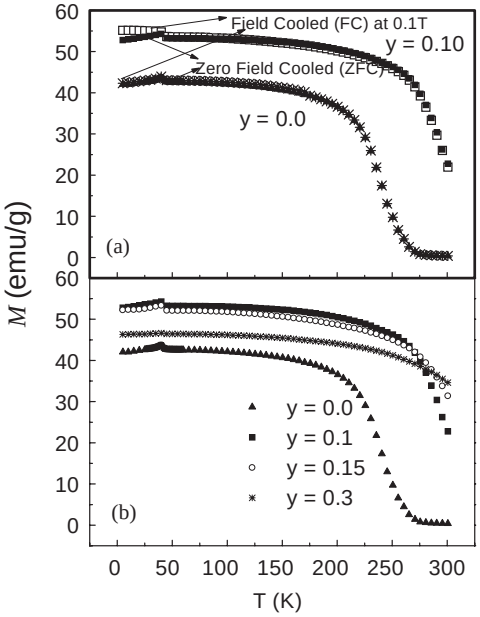

Fig. 3. (a) Zero field cooled (ZFC) and field cooled (FC) magnetization (M) at 0.1 T of $La_{0.7}Ca_{0.3-y}K_yMnO_3$ ($y = 0.0$ and 0.10) as a function of temperature. (b) Field Cooled $La_{0.7}Ca_{0.3-y}K_yMnO_3$ for different K concentrations (y) at 1000 G.

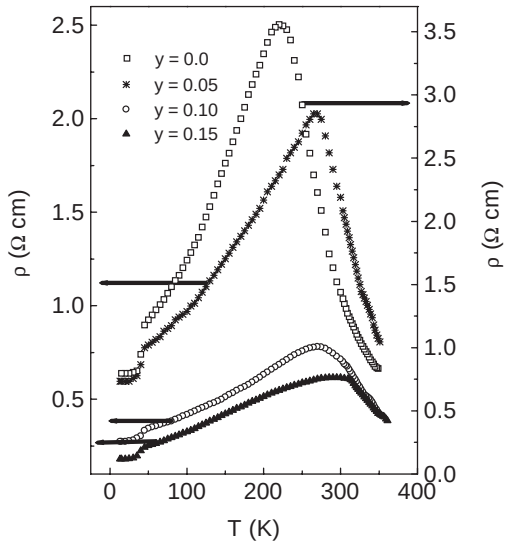

Fig. 4. Resistivity vs. temperature plot at zero magnetic field for different K concentrations.

magnetic clusters. This illustrates that there are possibly large ferromagnetic regions with multi-domain structure and magnetic clusters for $T < T_C$. With increasing magnetic field the magnetic moment value increases rapidly which can be attributed to the FM domain growth under applied field. For a similar kind of sample $La_{0.82}K_{0.08}MnO_{2.89}$ (LKMO), Das et al. [13] have shown that the resultant moment at 14 K is canted at an angle of $\sim$25–27° with respect to [0 0 1] crystallographic axis. The moment values obtained from the magnetization measurements are considerably lower than the values expected for fully aligned Mn spins, which could be due to the disorder induced by the lanthanum and oxygen vacancies. In the low temperature ferromagnetic phase, an anomaly in the magnetic moment is seen around 40 K for all the samples. Such an anomaly has also been reported earlier in composites of La–Ca–Mn–O with $SrTiO_3$ [14] as well as in some substituted La–Ca–Mn–O system. Ju and Shon [15] explained this anomaly on the basis of local microscopic magnetic inhomogeneties arising from the variation in the Mn oxidation state. On the other hand, in Ce doped La–Sr–Mn–O composites, this type of kink has been explained on the basis of the presence of the paramagnetic MnO_2 phase in the compound [16]. In the resistivity vs. temperature plot (Fig. 4 shown later) a corresponding drop in the resistivity is also observed for all the samples which further confirms the existence of this anomaly, which might be due to the same reason as mentioned above. It is also noticed that the strength of this anomaly decreases with increase of K concentration. Room temperature XRD study, however, does not indicate the presence of any paramagnetic MnO_2 phase in the sample. Approximately the same observed values of T_p and T_C (Table 2) indicate good quality of the samples with negligible grain boundary effect.

3.3. Transport properties

3.3.1. Magnetic field-dependent resistivity

All the samples with different K concentrations ($y = 0.0$, 0.05, 0.1, 0.15) show a metallic behavior (i.e. $d\rho/dT > 0$) at low temperatures and with rising temperature, a sharp MIT is seen at T_p, very close to the corresponding Curie temperature T_C

Table 2
Some important data of all the prepared samples from the magnetization and resistivity measurements made in presence and in absence of pulsed magnetic field

y	Mn^{4+}/Mn^{3+}	M (emu/g) ($B = 9.67$ kG) at $T = 300$ K	ρ (Ω-cm)		T_p (K) $B = 0$ T	T_C (K) $B = 0$ T
			$T = 300$ K	$T = T_p$		
0.0	0.428	3.949	1.44	3.24	220.0	220.0
0.05	0.538	15.686	1.58	2.03	280.0	278.5
0.10	0.666	39.903	0.71	0.78	291.5	290.5
0.15	0.818	47.387	0.55	0.61	299.5	295.9

of the sample (Fig. 4). The maximum resistivity ρ_{max} (peak value) decreases and T_p shifts to higher temperature as y increases (Table 2). This increase in conductivity with K doping is considered to be associated with the increase of the ratio of Mn^{4+}/Mn^{3+}, which in turn contribute to the enhancement of holes in the e_g band. This is in accordance with the suggestions made by others [8]. The values of Mn^{4+}/Mn^{3+}, with increasing y, obtained from the valency calculations (Table 2), supports this argument. The cation valency distribution can be represented as $La^{3+}_{1-x}Ca^{2+}_{x-y}K_y(Mn^{3+}_{1-(x+y)}Mn^{4+}_{x+y})O_3$. Hence, y amount increase of K ions will result in a $(x+y)$ amount increase in Mn^{4+} ions and consequently, a small amount of K doping will cause a large number of charge carriers and thus resistivity will be decreased. Rhombohedral distortion introduced by K doping is also an important contributor to the increase of T_C. Similar behavior is also observed with Na doped samples.

Temperature dependence of resistivity measured both in presence and in absence of pulsed magnetic field (maximum 3.2 T) on two typical samples with $y = 0.05$ and 0.15 are shown in Figs. 5a and b. The corresponding changes in %MR as a function of temperature is also shown in the same figure. Similar behavior is also obtained for other samples of this group. Application of pulsed magnetic field causes a significant decrease in the resistivity shifting the resistivity peak to the high temperature region. During the field pulse, the spins favorably orient themselves and consequently the charge carriers suffer less scattering showing a decrease in resistivity. Interestingly, we found that the thermal variation of resistivity measured under constant

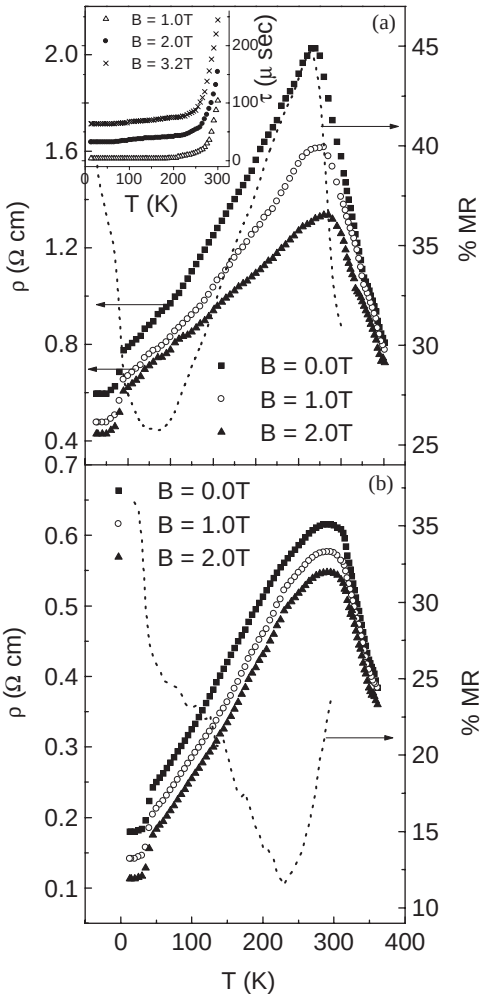

Fig. 5. Resistivity and % MR vs. temperature plot of (a) $La_{0.7}Ca_{0.25}K_{0.05}MnO_3$ and (b) $La_{0.7}Ca_{0.15}K_{0.15}MnO_3$ with different strengths of the pulsed magnetic fields. (a) Inset shows the relaxation time (τ) vs. temperature plot for the $y = 0.05$ sample.

DC field (1.5 T) is similar to that measured under pulsed field. However, some interesting temperature-dependent relaxation time behavior (time taken by the sample to return to the normal, i.e. zero field state after the pulsed field is switched off) is noticed. The plot of such relaxation time (ι) as a function of temperature for a typical sample (with $y = 0.05$) is shown in the inset of Fig. 5a. It is seen that the relaxation time (ι) depending on magnetic field strength is related to the magnetic spin ordering and falls sharply around T_C and remains almost constant in the low temperature FM phase (Fig. 5a inset). Similar results are also found for the other samples. Nearly constant value of (ι) in the ferromagnetic region indicates most ordered state behavior. In this regard it can be mentioned that, with the application of magnetic field or lowering the temperature below MIT, the FM clusters embedded in the paramagnetic matrix form a connecting path and hence percolation occurs. In the present system, due to momentary excitation (pulsed field), some spins in the paramagnetic matrix become polarized to increase the number of FM clusters, hence enhancing the conductivity. After the withdrawal of the field, these momentarily formed FM clusters will come back to its normal (unpolarized) state with an observed relaxation time (ι). Hence by measuring the relaxation time, the mixed phase tendency of these manganites can be well studied. We believe this is a more important physical issue, for our future investigation, that pulse field measurement could probe.

A plot of T_p vs. alkali metal ion concentration (y) shows almost exponential rise of T_p with increasing potassium content (Fig. 6). With increasing y, ρ_{max} first decreases sharply and then gradually approaches a minimum value (Fig. 6). This observation actually reflects that in the low doping regime ($y \leqslant 0.1$) the Mn^{4+}/Mn^{3+} ratio is favorable to ferromagnetism and hence extension of the FM-metallic phase is obtained. Further increase in the doping level, increases Mn^{4+} concentration and the antiferromagnetic superexchange interaction (Mn^{4+}–O–Mn^{4+}) becomes predominant over the DE interaction and conclusively increase of T_p and decrease of ρ_{max} with increasing y become much smaller. Magnetoresistance $(\Delta\rho/\rho_0) \times 100[= \{\rho(H = 0) - \rho(H)\}/\rho(H = 0) \times 100]$ is found to show a peak around their respective MIT temperature T_p. The dotted lines in Figs. 5(a) and (b) represent % MR of the samples with an applied magnetic field of 3.2 T.

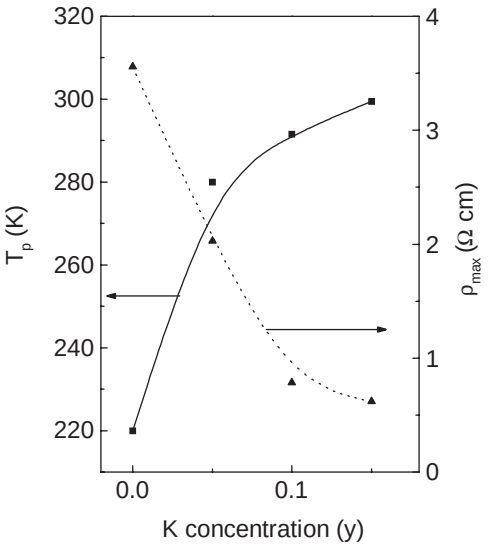

Fig. 6. Transition temperature T_p and maximum resistivity ρ_{max} vs. K concentration y plot for $B = 0$ T.

In the low temperature ferromagnetic metallic phase, the temperature dependence of the resistivity for all the samples both in presence and in absence of the pulsed magnetic field can be well fitted (Fig. 7) by the equation of the form

$$\rho(T) = \rho_0 + \rho_2 T^2, \quad (1)$$

where the temperature independent part ρ_0 is the resistivity due to domain, grain boundary and other temperature independent scattering mechanism [17,18]. Some authors have explained the $\rho_2 T^2$ by the electron–electron scattering process [18] but following Mott [19] $\rho \sim T^2$ behavior in a ferromagnet is due to magnon scattering. We also believe that the spin scattering cannot be neglected in the low T regime as the measured data can be best explained by electron-spin scattering. The best-fit parameters obtained from fitting the low temperature metallic part of the resistivity data with Eq. (1) are shown in Table 3. As expected, the temperature independent term (ρ_0) for all the

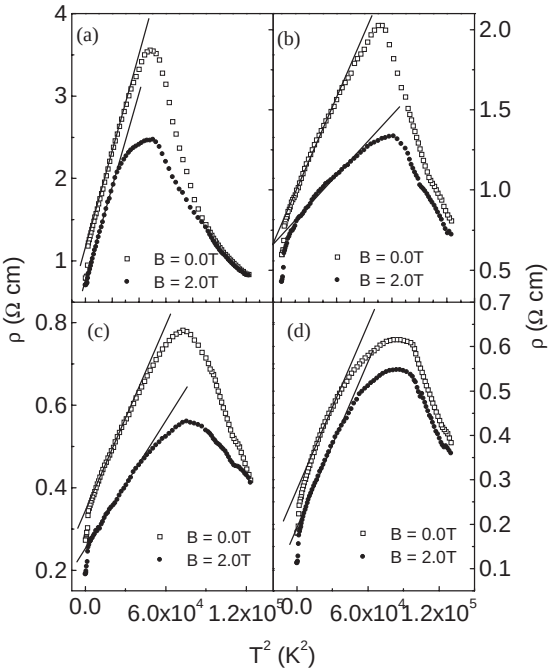

Fig. 7. Linear fit of the low temperature (FM region) resistivity data with T^2 term (Eq. (1)) for the sample (a) $y = 0.0$, (b) $y = 0.05$, (c) $y = 0.1$ and (d) $y = 0.15$.

Table 3
The values of the parameters ρ_0 and ρ_2 of all the samples obtained from fitting the low temperature ($T < T_p$) resistivity data with Eq. (1) in presence and in absence of magnetic field

y	ρ_0 (Ω-cm)		ρ_2 (Ω-cm K^{-2})	
	$B = 0.0$ T	$B = 2.0$ T	$B = 0.0$ T	$B = 2.0$ T
0.0	1.13	0.87	6.09×10^{-5}	3.40×10^{-5}
0.05	0.79	0.70	1.86×10^{-5}	1.16×10^{-5}
0.10	0.35	0.27	6.81×10^{-6}	5.92×10^{-6}
0.15	0.26	0.20	6.22×10^{-6}	5.83×10^{-6}

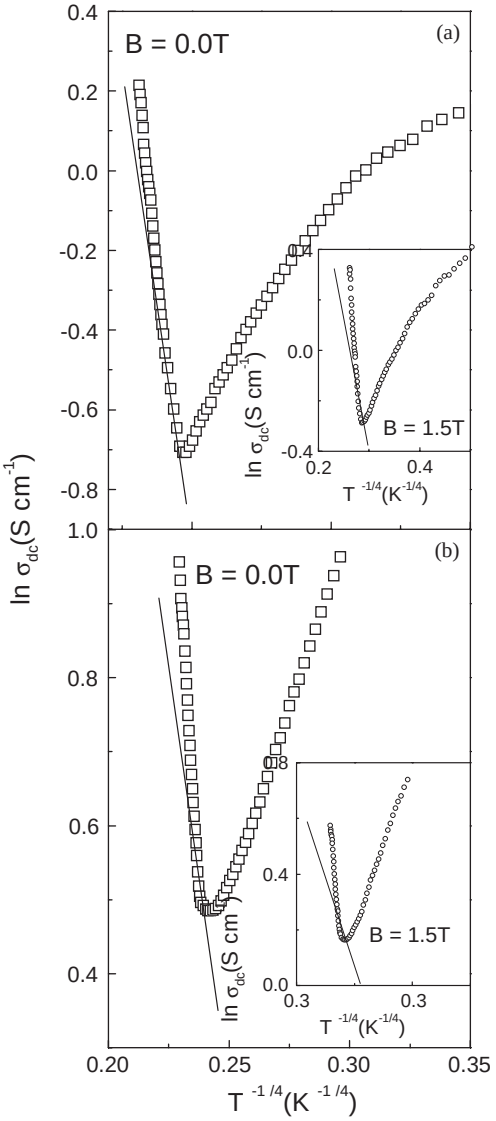

Fig. 8. Variation of conductivity log σ_{dc} as a function of $T^{-1/4}$ (Eq. (2)) for (a) $y = 0.05$ with and (b) $y = 0.15$ with $B = 0$ T. Insets show the plot with $B = 1.5$ T. Solid lines are the best-fit to the VRH model (Eq. (2)).

polycrystalline samples decreases significantly with the magnetic field but the influence of the magnetic field on the ρ_2 term is comparatively small. It is likely that the mechanism responsible for MR in the system, is the influence of the magnetic field on the ordering of magnetic domains. As the pulsed magnetic field strength increases, the size of the domain boundary decreases and ρ_0 becomes smaller [20]. The decrease of ρ_2 in a magnetic field is due to the suppression of spin fluctuation in the applied magnetic field (proportional to $B^{-1/3}$) [18].

All the resistivity data, above the transition temperature T_p, have earlier [21] been fitted with variable range hopping (VRH) of charge carriers. Recently, Viret et al. [22] and Pal et al. [10] have applied VRH conduction mechanism in systems

like La–Ca–Mn–O, La–Mn–O, La–Pb–Mn–O, etc. at higher temperatures above T_p. Similarly our data between T_p and 320 K also fit the VRH model quite well. This model in three-dimensional cases, can be written as

$$\sigma_{dc} = \sigma_0 \exp[-(T_0/T)]^{1/4}, \quad (2)$$

where T_0 is a constant [$= 18\alpha^3/k_B N(E_F)$], α is the electron wave function decay constant, k_B is Boltzman's constant and $N(E_F)$ is the density of states at the Fermi level which can be calculated from the slope of the plot of $\log \sigma_{dc}$ vs. $T^{-1/4}$ curves [shown in Figs. 8(a) and (b)]. The best-fit occurs with $T_0 \sim 10^6$ for both La–Ca–Mn–O and La–Ca–K–Mn–O which is in good agreement with the previously reported results [10]. We have also calculated T_0 for different samples in presence of magnetic fields. T_0 is found to decrease with the increasing magnetic field strength. From Eq. (2) we also estimated $N(E_F)$ (Table 4) using $\alpha = 2.22\,\mathrm{nm}^{-1}$ as used by Pal et al. [10]. The value of $N(E_F)$ are comparable to those obtained by Coey et al. [21] ($N(E_F) \sim 4 \times 10^{22}/\mathrm{eV\,cm}^3$ for La–Ca–Mn–O system) and Pal et al. [10] ($N(E_F) \sim 5.99 \times 10^{22}/\mathrm{eV\,cm}^3$ for La–Pb–Mn–O system). The $N(E_F)$ value for the present sample is found to be increasing with the application of magnetic field. It is noticed that for the K doped sample $N(E_F)$ is much higher than that of the undoped sample indicating appreciable increase in the number of charge carriers and consequently showing an increase in the conductivity of the K doped sample. Also the application of magnetic field decreases the localization length which in turn increases the number of delocalized charge carriers causing increased $N(E_F)$.

It should be mentioned here that the VRH model could not be extended to fit well the data above 320 K (between 320 and 350 K). Recently, it has been shown by Banerjee et al. [11] that the conductivity data between T_p and $\theta_D/2$ (θ_D being the Debye temperature) can only be well fitted with VRH model. The high temperature ($T > \theta_D/2$) resistivity data of the Cr doped and undoped La–Pb–Mn–O manganite samples can be well fitted with the thermally activated small polaron hopping (SPH) model. Similar behavior is also exhibited by the present K doped system. For the samples with higher T_p values (like the present samples), the VRH region is small. So it is rather difficult to judge which of the two models is most appropriate. It is, however, noticed that the high temperature ($T > \theta_D/2$) conductivity data between 320 and 350 K for the K doped samples (Figs. 9(a) and (b)) better fit the SPH model of Mott viz. $\rho/T = \rho_\alpha \exp(E_p/k_B T)$, where $\rho_\alpha = [k_B/\nu_{ph} N e^2 R^2 C(1-C)] \exp(2\alpha R)$ where N is the number of ion sites per unit volume (obtained from the density data), R is the average intersite spacing obtained from the relation $R = (1/N)^{1/3}$, E_p is the activation energy for hopping conduction estimated from the conductivity data, C is the fraction of sites occupied by a polaron, α is the electron wave function decay constant obtained from fitting the experimental conductivity data, ν_{ph} is the optical phonon frequency (estimated from the relation $h\nu_{ph} = k_B\theta_D$). We have replotted the resistivity curve as $\ln(\rho/T)$ vs. $1/T$ and from the slope of the curve the activation energy E_p is estimated (Table 4). The activation energies are found to decrease with increasing K doping

Table 4
Values of the density of states (DOS) at the Fermi level ($N(E_F)$), activation energies from resistivity and TEP data (E_p and E_S), polaron hopping energy (W_H) and the constant (α') of Eq. (4) both in absence and in presence of a magnetic field (1.5 T)

y	$N(E_F) \times 10^{-21}$ ($\mathrm{eV}^{-1}\,\mathrm{cm}^{-3}$)		E_p (meV)		E_S (meV)		W_H (meV)		α'	
	$B = 0$ T	1.5 T	$B = 0$ T	1.5 T	$B = 0$ T	1.5 T	$B = 0$ T	1.5 T	$B = 0$ T	1.5 T
0.0	0.380	1.701	116.3	91.95	13.16	9.38	103.2	82.57	−0.61	−0.45
0.05	0.404	0.636	110.7	91.23	9.89	9.82	100.9	81.40	−0.50	−0.49
0.10	0.822	2.705	99.07	88.46	8.38	8.32	90.69	80.15	−0.45	−0.43
0.15	1.265	4.609	92.52	82.14	8.01	7.81	84.50	74.33	−0.42	−0.41

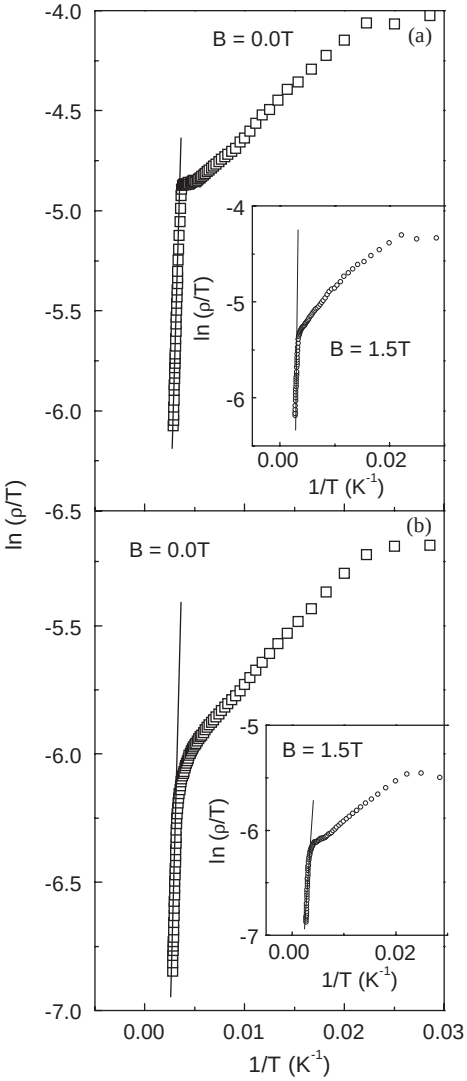

Fig. 9. Variation of $\log(\rho/T)$ as a function of $1/T$ for (a) $y = 0.05$ with and (b) $y = 0.15$ with $B = 0\,\mathrm{T}$. Insets show the plot with $B = 1.5\,\mathrm{T}$. Solid lines are the best-fit to the Mott's SPH model (see text).

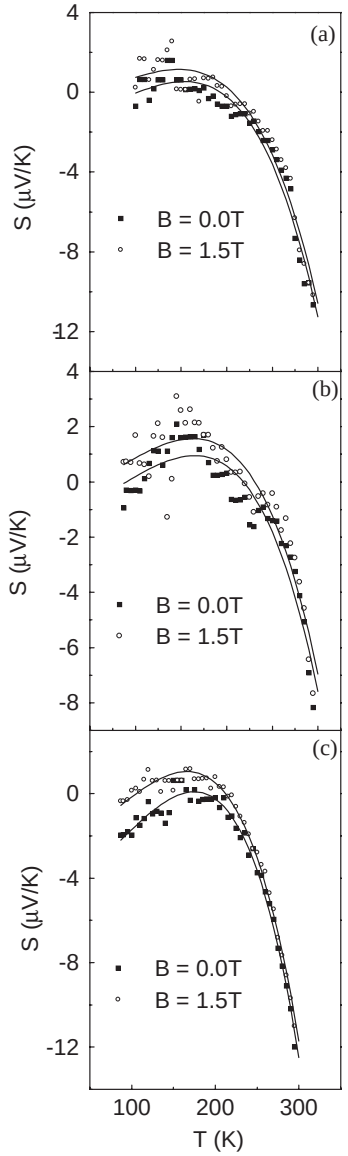

Fig. 10. Temperature and magnetic field ($B = 1.5\,\mathrm{T}$)-dependent Seebeck coefficient (S) of three different samples $La_{0.7}Ca_{0.3-y}K_yMnO_3$ with (a) $y = 0.05$, (b) 0.1 and (c) 0.15. Solid lines are the best-fit to the Eq. (3).

concentration and with the application of magnetic field. Actually, due to hole doping in the e_g band the delocalization of charge carriers occurs and hence the energy required to liberate a free carrier is reduced. Application of magnetic field enhances this delocalization thereby reducing the activation energy further.

3.3.2. *Magnetic field-dependent thermoelectric power (TEP)*

Magnetic field ($B = 0-1.5\,\mathrm{T}$)-dependent thermoelectric power (Seebeck coefficient, S) of the K doped $La_{0.7}Ca_{0.3-y}K_yMnO_3$ ($0.0 \leqslant y \leqslant 0.15$) system measured in the temperature range 80–300 K also

supports the conductivity results discussed above. Fig. 10 displays the temperature-dependent thermoelectric power of the samples with different values of $y = 0.05$, 0.1 and 0.15 in presence (1.5 T) and absence of magnetic field. All the K doped samples show a change in the sign of Seebeck coefficient. With the increase of K ions, S tends towards positive value. This increasing trend of S is seen upto $y = 10\%$ which can be attributed to the increase in the number of Mn^{4+} ions due to increasing hole concentration (as discussed above). For $y = 0.15$, the S value is marginally lower but shows the same nature as the other two samples. Addition of K ions causes more hole doping centers, which are localized in character and hence S value increases. This large value of thermopower arising from hole localization may occur due to the narrowing of e_g band and it also indicates distortion of the Fermi surface.

For all the samples, it is observed that with the application of magnetic field ($B = 1.5$ T), S value increases at low temperature and the difference between the two values $\Delta S[= S(0) - S(1.5)]$ decreases near T_p (where $S(0)$ and $S(1.5)$ are the value of S in zero and 1.5 T field). This indicates that spin ordering that occurs under magnetic field, increases thermopower of the present manganite samples. The temperature dependence of S below T_p can be fitted as before [23] with the relation of the form

$$S = S_0 + S_{1.5}T^{1.5} + S_4T^4, \quad (3)$$

where S_0 is a constant term having no physical origin. The low temperature (FM phase below T_p), TEP data of the samples (with $y = 0.0-0.15$) are well fitted with Eq. (3) (some are shown in Figs. 10a–c). From the corresponding fitting parameters shown in Table 5, we find $S_{1.5} \gg S_4$ which suggests that at low temperatures, S is mainly governed by the second term in Eq. (3) arising due to electron–magnon scattering contribution. It is also shown above from the low temperature (FM phase) resistivity data (Eq. (1)) that the electron–magnon scattering process dominates the conduction mechanism in the alkali metal Na-doped manganites. Therefore, from the TEP measurements also, it is reconfirmed that electron–magnon scattering process is predominant in the low temperature FM phase. Decrease of electron–magnon scattering term ($S_{1.5}T^{1.5}$) under magnetic field suggests that spins get favorably oriented under magnetic field and hence electron-spin scattering possibility diminishes and the system behaves like a metal. But in the low temperature metallic phase (below T_p), the exchange coupling strength increases leaving the electrons more delocalized and this makes the system magnetic (ferro- or antiferromagnetic, depending on concentration, strength of exchange interaction). At high temperatures the T^4 term (spin wave fluctuation contribution) cannot be neglected and this term actually fits the data (with Eq. (3)) over the high temperature region. The parameter S_0 (Eq. (3)) is found to increase in presence of magnetic field. However, the interdependency of the parameters S_0, $S_{3/2}$, etc. is not well known and needs further study.

More interesting result is obtained from the high temperature regime ($T > \theta_D/2$) TEP data where there is disorder and localization. In this region

Table 5
The values of the parameters S_0, $S_{1.5}$ and S_4 obtained from fitting the low temperature (ferromagnetic metallic phase) thermoelectric power (TEP) data of $La_{0.7}Ca_{0.3-y}K_yMnO_3$ ($y = 0-0.15$) with Eq. (3) both in presence ($B = 1.5$ T) and in absence ($B = 0$) of magnetic field (B)

y	S_0 (μV/K)		$S_{1.5}$ (μV/K$^{2.5}$)		S_4 (μV/K^5)	
	$B = 0.0$ T	1.5 T	$B = 0.0$ T	1.5 T	$B = 0.0$ T	1.5 T
0.00	−3.84	−3.71	2.34×10^{-3}	2.30×10^{-3}	-4.10×10^{-9}	-5.69×10^{-9}
0.05	−1.66	−0.60	1.85×10^{-3}	1.57×10^{-3}	-2.37×10^{-9}	-2.24×10^{-9}
0.10	−1.38	−0.64	1.76×10^{-3}	1.70×10^{-3}	-1.89×10^{-9}	-1.86×10^{-9}
0.15	−4.72	−2.59	3.34×10^{-3}	2.72×10^{-3}	-3.09×10^{-9}	-2.87×10^{-9}

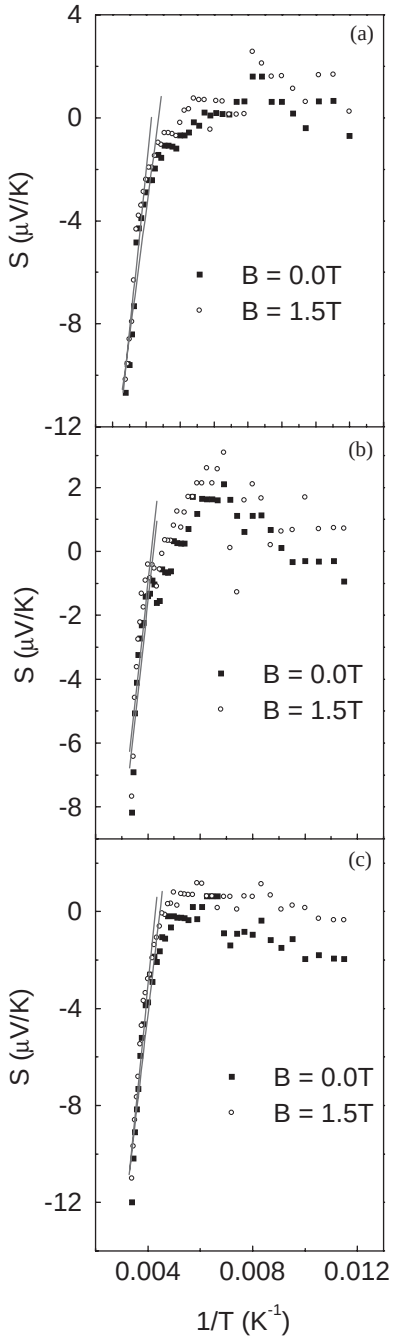

Fig. 11. The Seebeck coefficient S vs. $1/T$ plot for four different $La_{0.7}Ca_{0.3-y}Na_yMnO_3$ samples with (a) 0.05, (b) 0.1 and (c) 0.15. Solid lines are the best-fit to the Mott's model (Eq. (4)).

TEP data fits excellently with Mott's well-known equation of Seebeck coefficient based on polaron hopping, viz.

$$S = k_B/e\left[E_S/k_BT + \alpha'\right], \tag{4}$$

where E_S is the activation energy obtained from the TEP data and α' is a constant related to the kinetic energy ($= k_BT\alpha'$) of the polarons (carriers). For $\alpha' < 1$ small polaron hopping conduction occurs, while for $\alpha' > 2$ the conduction involves large polarons. Fig. 11 gives the S vs. $1/T$ plots for all the samples both in presence and in absence of magnetic field. Solid line gives the best-fit of the experimental data with Eq. (4). From the slope of S vs. $1/T$ curves, we obtain the values of activation energy E_S of the samples shown in Table 4. The constant α' is obtained from the intercept of the plotted curves (Table 4). The estimated values of α' (from Eq. (4)), indicated $\alpha' < 1$ for both zero and 1.5 T magnetic field. Therefore, small polaron hopping conduction mechanism is also supported by the high temperature ($T > T_p$) TEP data.

With the application of magnetic field, we noticed (Table 4) that polaron hopping energy ($W_H = E_p - E_S$) and polaron binding energy decreases. This indicates that with increasing K concentration the system becomes more metallic and hence the polaronic conduction regime is gradually converted to electronic conduction regime. This is an interesting observation from the study of K doped manganite system. Similar result is also obtained with Na doped system [24].

4. Conclusion

In conclusion, magnetic and magnetotransport properties of $La_{1-x}Ca_{x-y}K_yMnO_3$ for $x = 0.3$ and $0 \leqslant y \leqslant 0.15$ measured under pulsed magnetic field (0.0–3.2 T) shows monovalent alkali metal K doping in La–Ca–Mn–O system drives the system towards higher conductivity and higher Curie and metal–insulator transition temperature region. The low temperature resistivity and TEP data signify the importance of electron–magnon scattering whereas the high temperature transport properties are mainly governed by the small polaron hopping

mechanism. Since both T_C and T_p can be varied around room temperature only by little increase of K at the Ca site, the present K doped system might be a potential candidate for device applications. We also like to state that the pulsed field technique, used in the present measurement, is a convenient technique, which would be very useful for measuring the magnetotransport properties of rare earth manganites, thin films, superconducting and other related materials of current interest. The temperature, magnetic field dependent relaxation time (ι) observed in pulsed field may also be used to determine the field-dependent spin ordering in the low temperature ferromagnetic phase. The relaxation time is also found to be dependent of the grain size of the sample. The pulsed field technique might be an important tool for elaborate investigation of all these features in the future.

Acknowledgements

The authors are grateful to the Department of Science and Technology, Government of India, for financial support. One of the authors (BKC) is also grateful to the NSC, Taiwan for the partial financial support during his stay at the Department of Physics, NSYSU, Taiwan.

References

[1] C. Zener, Phys. Rev. 82 (1951) 403.
[2] A.J. Millis, P.B. Littlewood, B.I. Shraiman, Phys. Rev. Lett. 74 (1995) 5144.
[3] J.M. Gonzalez-Calbet, E. Herrero, N. Rangavittal, J.M. Alonso, J.L. Martinez, M. Vallel-Kegi, J. Solid State Chem. 148 (1999) 158;
N. Abdelmoula, K. Guidara, A. Cheikhrouhou, E. Dhahri, J.C. Joubert, J. Solid State Chem. 151 (2000) 139.
[4] J.A.M. van Roosmalen, P. van Vlaanderen, E.H.P. Cordfunke, J. Solid State Chem. 114 (1995) 516.
[5] C. Boudaya, L. Laroussi, E. Dhahri, J.C. Joubert, A. Cheikhrouhou, J. Phys.: Condens. Matter 10 (1998) 7485.
[6] G.H. Rao, J.R. Sun, K. Bärner, N. Hamad, J. Phys.: Condens. Matter 11 (1999) 1523.
[7] N. Abdelmoula, A. Cheikhrouhou, L. Reversat, J. Phys.: Condens. Matter 13 (2001) 449.
[8] S. Roy, Y.Q. Guo, S. Venkatesh, N. Ali, J. Phys.: Condens. Matter 13 (2001) 9547.
[9] M. Date, High Field Magnetism, North-Holland, Amsterdam, 1983.
[10] S. Pal, A. Banerjee, E. Rozenberg, B.K. Chaudhuri, J. Appl. Phys. 89 (2001) 4955.
[11] Aritra Banerjee, S. Pal, B.K. Chaudhuri, J. Chem. Phys. 115 (2001) 1550.
[12] S. Bhattacharya, A. Banerjee, S. Pal, R.K. Mukherjee, B.K. Chaudhuri, J. Appl. Phys. 93 (2003) 356;
S. Bhattacharya, A. Banerjee, S. Pal, P. Chatterjee, R.K. Mukherjee, B.K. Chaudhuri, J. Phys.: Condens. Matter 14 (2002) 10221.
[13] A. Das, M. Sahana, S.M. Yusuf, L. Madhav Rao, C. Shivkumara, M.S. Hegde, Mater. Res. Bull. 35 (2000) 651.
[14] D. Das, P. Chowdhury, R.N. Das, C.M. Srivastava, A.K. Nigam, D. Bahadur, J. Magn. Magn. Mater. 238 (2002) 178;
D.K. Petrov, L. Krusin-Elbaum, J.Z. Sun, C. Field, P.R. Duncombe, Appl. Phys. Lett. 75 (1999) 995.
[15] H.L. Ju, H. Sohn, J. Magn. Magn. Mater. 167 (1997) 2041.
[16] J.R. Gebhardt, S. Roy, N. Ali, J. Appl. Phys. 85 (1999) 5390.
[17] G. Jeffrey Synder, R. Hiskes, S. Dicarolis, M.R. Beasley, T.H. Geballe, Phys. Rev. B 54 (1996) R15606.
[18] A. Urushibara, Y. Moritomo, T. Amira, A. Asamitsu, G. Kido, Y. Tokura, Phys. Rev. B 51 (1995) 14103.
[19] N.F. Mott, Metal–Insulator Transitions, Taylor & Francis, London, 1974.
[20] P. Schiffer, A.P. Ramirez, W. Bao, S.W. Cheong, Phys. Rev. Lett. 75 (1995) 3336.
[21] J.M.D. Coey, M. Viret, L. Ranno, Phys. Rev. Lett. 75 (1995) 3910.
[22] M. Viret, L. Ranno, J.M.D. Coey, Phys. Rev. B 55 (1997) 8067.
[23] S. Aritra Banerjee, S. Pal, H.D. Bhattacharya, B.K. Yang, Chaudhuri, Phys. Rev. B 64 (2001) 104428.
[24] S. Bhattacharya, S. Pal, A. Banerjee, H.D. Yang, B.K. Chaudhuri, J. Chem. Phys. 119 (2003) 3972.